Tough and Elastic Cellulose Composite Hydrogels/Films for Flexible Wearable Sensors

Tiangang Yang,<sup>a</sup> Shaohao Lu,<sup>b</sup> Honglin Zhu,<sup>c</sup> Antonios Patetsos,<sup>a</sup> Emma McDonald,<sup>a</sup> Matthew D.

Mellor, a Yangchao Luo, James F. Rusling, a,e,f,g Xueju Wang, b,d,e,\* Jie Hea, d,e,\*

<sup>a</sup> Department of Chemistry, <sup>b</sup> Department of Materials Science and Engineering, <sup>c</sup> Department of

Nutritional Sciences, and <sup>d</sup> Polymer Program, <sup>e</sup> Institute of Materials Science, University of Connecticut,

Storrs, CT 06269, USA.

<sup>f</sup> Department of Surgery and Neag Cancer Center, UConn Health, Farmington, CT 06030.

<sup>g</sup> School of Chemistry, National University of Ireland at Galway, Galway, Ireland. H91 TK33.

Email: Xueju.wang@uconn.edu (XW) and Jie.he@uconn.edu (JH)

**Abstract:** 

Cellulose and its composites, despite being abundant and sustainable, are typically brittle with very low flexibility/stretchability. This study reports a solution processing method to prepare porous, amorphous and elastic cellulose hydrogels and films. Native cellulose dissolved in water-ZnCl<sub>2</sub> mixture can form ionic gels through *in situ* polymerization of acrylic acid (AA) to poly(acrylic acid) (PAA). The addition of up to 30 vol% of AA does not change the solubility of cellulose in the water-ZnCl<sub>2</sub> mixture. After polymerization, the formation of interpenetrated networks, resulting from chemical cross-linking of PAA and the ionic/coordination binding among cellulose/PAA and ZnCl<sub>2</sub>, gives rise to strong, transparent, ionically conductive hydrogels. These hydrogels can be used for wearable sensors to detect mechanical deformation under stretching, compression and bending. Upon removal of ZnCl<sub>2</sub> and drying the gels, semi-transparent amorphous cellulose composite films can be obtained with a Young's Modulus up to 4 GPa. The rehydration of these films leads to the formation of tough, highly elastic composites. With a water content of 3-10.5%, cellulose-containing films as strong as paper also show typical characteristics of elastomers with elongation up to 1300%. Such composite films provide an alternative solution to resolving materials sustainability of natural polymers without compromising their mechanical properties.

**Keywords:** cellulose hydrogels, cellulose composite films, elasticity, tough elastomers, strain sensor, wearable sensor.

1

### 1. Introduction

Cellulose and its derivatives, as the most abundant organic materials on earth, have received considerable attention for their sustainability, biodegradability and biocompatibility in bio-related applications, such as healthcare products (biosensors<sup>1-4</sup> and actuators<sup>5-8</sup>), tissue engineering<sup>9-11</sup> and agriculture. 12-14 As a linear polysaccharide composed of D-glucose linked through glycosidic bonds, cellulose contains three hydroxyl groups in each repeating unit and forms highly crystalline microcrystals in plants and/or shell animals due to strong interchain hydrogen bonding. Unprocessed cellulosic materials typically exhibit high brittleness, low flexibility/stretchability, as well as limited optical clarity, making them unsuitable for versatile bio-related uses. For example, paper made of cellulose microfibers has a typical elongation at break of <3% and tensile strength of 1-30 MPa. 15 Regenerated cellulose also has low fracture strength and poor mechanical elasticity due to weakly entangled microcrystals/nanocrystals and the persistence of robust hydrogen bonds resulting from incomplete chemical conversion to hydroxyl groups. Thus, glycerol and glycol are commonly utilized as additive plasticizers in regenerated cellulose to reduce interchain interactions and improve the mechanical robustness (both tensile strength and toughness). With about 10 wt% loading of glycerol, cellulose-based fiber can become thermoplastics with elongation at break close to 10%. <sup>16</sup> Ionic liquids as another example can strongly solvate the crystalline domains of cellulose to induce loosely packed cellulose chains that can effectively dissipate energy and provide high elasticity.<sup>17</sup> With the high flexibility and stretchability of functional cellulose composites, cellulose-based strain sensors can detect various human movements, encompassing both large-scale actions like joint bending and small-scale physiological activities such as breathing and pulse. 18 Additionally, strain sensors fabricated with biocompatible and transparent cellulose composites enable dressing and direct inspection of the skin surface, facilitating continuous monitoring of wound healing status. 19 The transparent strain sensors can be further integrated with optical sensors, such as fluorescent pH or glucose indicators, into multifunctional sensing systems to provide comprehensive insight into patients' physical conditions. 20, 21

On the other hand, there has been an ongoing effort to search for environmentally friendly and low-cost solvent systems to process cellulose ideally in water. In the past three decades, new solvent systems, *e.g.*, N-methylmorpholine-N-oxide monohydrate, <sup>22</sup> ionic liquid, <sup>23</sup> NaOH/urea, <sup>24</sup> and molten salt hydrates (examples are LiCl·5H<sub>2</sub>O, <sup>25</sup> LiClO<sub>4</sub>·3H<sub>2</sub>O, <sup>26</sup> ZnCl<sub>2</sub>·3H<sub>2</sub>O, <sup>25</sup>, <sup>27</sup> and AlCl<sub>3</sub>/ZnCl<sub>2</sub>·4H<sub>2</sub>O<sup>28</sup>), have been developed to dissolve and process cellulose. Among various molten salt hydrates, ZnCl<sub>2</sub>·3H<sub>2</sub>O is an inexpensive solvent to dissolve cellulose directly in water at room temperature. <sup>27</sup> Those solvent systems

have been extensively studied to prepare cellulose-based hydrogels. Among them, molten salt hydrates as solvents for cellulose are not only ionically conductive but also act as an efficient antifreezer to broaden the serving temperature of hydrogels by lowering the freezing point of water.<sup>29</sup> For example, cellulose dissolved in an aqueous solution of ZnCl<sub>2</sub>/CaCl<sub>2</sub> could form hydrogels,<sup>29</sup> where Ca<sup>2+</sup> ions acted as a gelation agent in the presence of glycerol. This hydrogel is ionically conductive even at -70 °C. However, upon removal of water, those cellulose-containing hydrogels often result in the formation of brittle films without elasticity.<sup>30</sup> The regenerated cellulose film from ZnCl<sub>2</sub>·3H<sub>2</sub>O as an example shows a tensile strength of 31 MPa with an elongation at breaking of less than 5%.<sup>28</sup> Additionally, cellulose-based hydrogels can also be prepared via *in situ* polymerization of water-soluble monomers in the cellulose solution. Polyacrylamide, as an example, can form interpenetrating polymer network with cellulose dissolved in NaOH/urea through *in situ* polymerization of acrylamide.<sup>31</sup> The extensive hydrogen bonding network largely improved the mechanical strength of hydrogels. Yet, most of hydrogels are rather weak mechanically with low tensile strength of 1-100 kPa and modulus < 1 MPa.<sup>31</sup>

To further enhance the processability, optical transparency and mechanical properties of cellulosic materials, we report a solution processing method to fabricate porous and amorphous cellulose hydrogels and films. The key idea is to simply use a polymer network that strongly interacts with cellulose to weaken its interchain interaction of cellulose through hydrogen bonding competition, where amorphous cellulose domains with loosely packed chains can improve their elasticity. This process was carried out by dissolving native cellulose in ZnCl<sub>2</sub> ·3H<sub>2</sub>O and first preparing cellulosic hydrogels through in situ polymerization with acrylic acid (AA). Zn<sup>2+</sup> ions not only break interchain hydrogen bonding and form strong coordination with cellulose to provide the solubility of cellulose in water; but also bind with the monomer AA through charge interaction. After polymerization, cellulose chains and poly(acrylic acid) (PAA) bridged by Zn<sup>2+</sup> ions can construct robust ionic hydrogels with high toughness resistant to both mechanical stretching and compression. Even after the removal of ZnCl<sub>2</sub>, the cellulose/PAA composite films still show highly elastic characteristics with an elongation of up to 1300% and a tensile strength of ca. 10-15 MPa, nearly as strong as printing paper but elastic as rubber bands. Furthermore, we demonstrate cellulose/PAA hydrogels and films as conducive electrodes in capacitive strain sensors. Our cellulosebased strain sensors demonstrate good sensing performance, high optical clarity, and deformability, offering versatility for biomedical applications.

### 2. Experimental

### 2.1 Chemicals and Materials

All chemicals and reagents were purchased from commercial sources and used as received. Cellulose microcrystalline powder (degree of polymerization  $\leq$ 350) was obtained from Thermo Scientific. Zinc chloride anhydrous (98+%, crystalline solid) was purchased from Alfa Aesar. AA ( $\geq$ 99.0%), N,N'-methylene bis(acrylamide) (MBA) (99%), and ammonium persulfate (APS) (ACS reagent,  $\geq$ 98.0%) from Sigma Aldrich. Deionized water (High-Q, Inc. 103S Stills) with a resistivity of >10.0 M $\Omega$  was used in all experiments. Double sided tape very high bond (VHB) Tape 4905, adhesive transfer tape (468MP) and polyimide film tape 5413 were obtained from 3M Company.

# 2.2 Dissolution of Cellulose

1.5 g of cellulose microcrystalline powder was first dispersed in 48.5 g of ZnCl<sub>2</sub>-water (70 wt% of ZnCl<sub>2</sub>) solution at ambient temperature under stirring. The dispersed suspension was then heated to 65 °C in a water bath for 2 h until a uniform transparent solution was formed shown in Figure 1a. This gave a 3 wt% cellulose stock solution. Cellulose stock solutions at different concentrations of 1-5 wt% cellulose were prepared similarly.

# 2.3 Hydrogels and Films of Cellulose/PAA through in situ Polymerization

In brief, 1.75 g of AA and 9.0 mg of MBA were added into 10 g of 3 wt% cellulose solution. The mixture was sonicated for about 10 min to form a uniform and clear solution. 100 µL of APS solution (50 mg/mL in water) was then quickly added into the above solution. The solution was degassed and transferred to a petri dish. After polymerization for 2 h, a transparent hydrogel was formed. The sample was denoted as C2.5/PAA14.9, where the number represents the weight ratio of each component in the gel. Ionic hydrogels with different amounts of cellulose (0.8-4.3 wt%) and PAA (9.0-16.7 wt%) were also prepared with the detailed compositions summarized in Table 1. The ionic gel was also prepared in different shapes and thicknesses for other measurements as noted later.

To remove ZnCl<sub>2</sub>, fresh-made hydrogels were immersed in a large amount of deionized water and stirred for 12 h. The water was refreshed every 2 h. After washing, the gel was dried under vacuum at 40 °C overnight. Uniform and semi-transparent films were acquired after drying.

**Table 1.** Preparation of ionic hydrogels and their mechanical analysis.

Samples	AA Content	Cellulose	Young's	Elongation at	Toughness
	(wt%)	Content (wt%)	Modulus (kPa)	breaks	$(MJ/m^3)$
C0.8/PAA14.9	14.9	0.8	103.9±11.1	2.9±0.1	4.7±1.2
C1.7/PAA14.9	14.9	1.7	163.2±14.5	2.5±0.1	7.4±1.6
C2.5/PAA14.9	14.9	2.5	332.7±23.8	3.6±0.3	39.7±5.6
C3.4/PAA14.9	14.9	3.4	349.1±29.2	3.0±0.1	28.0±4.8
C4.3/PAA14.9	14.9	4.3	208.6±20.6	3.2±0.2	17.9±2.9

### 2.4 Fabrication and Characterizations of Sensors

Fabrication of gel strain sensors: The C2.5/PAA14.9 gel was cut into two rectangular pieces, each measuring 7 mm × 21 mm, to serve as the stretchable electrodes for the capacitive strain sensor. A dielectric layer (VHB 4905, 3M) was sandwiched between two layers of C-2.5/PAA-14.9 gel for capacitive sensing. Two conductive wires were attached to the ends of the C2.5/PAA14.9 electrodes as interconnects to external equipment for data acquisition. Finally, the sensor was encapsulated with two additional layers of VHB 4905 tape as barriers to fluids.

Fabrication of gel pressure sensors: The C2.5/PAA14.9 gel was cut into a circular shape with a diameter of 15 mm. Two pairs of conductive wires were positioned orthogonally on the two sides of the circular Cellulose-2.5/PAA-14.9 gel. The sensor was assembled by encapsulating the gel with polyimide film tapes (PI film tape 5413, 3M) on both sides.

Fabrication of film strain sensors: The bending sensors were established similarly as strain sensors where the outer encapsulation layers were replaced by a thinner acrylic adhesive (3M, 468MP, thickness of 130  $\mu$ m) and C2.5/PAA14.9 film (~10% water content) was used for capacitive sensing.

Characterization of the sensors: The performance of both the pressure and strain sensors was evaluated by applying cyclic mechanical loading using a mechanical tester (Univert, CellScale). For the pressure sensor, compressive pressure (120 kPa) was applied and held for 15 seconds, then released for 15 seconds; the process was repeated for a total of 20 cycles. The strain sensor was stretched to a maximum strain of 30% in 5 seconds and then released to its initial state in 5 seconds; the process was repeated for 10 cycles.

During the cyclic loading, resistance and capacitance values were recorded for the pressure sensor and the strain sensor, respectively, using an LCR meter (IM3533, Hioki).

#### 2.5 Characterizations

The UV-vis results were collected on a Cary 60 spectrometer. For the titration experiment, 1.0 mL ZnCl<sub>2</sub>cellulose mixture was titrated with 25 µL of water or AA in a 3 mL quartz cuvette under transmission mode. The transmittance was measured after stirring the solution for 2 min. To measure the transmission of the ionic hydrogels, the gel was directly mounted on the light path of the spectrometer. The Fouriertransform infrared (FTIR) spectroscopy of different samples was obtained on a Fisher Thermo Nicolet iS 50 Spectrometer equipped with an iD7 ATR accessory. To measure IR spectra, ZnCl<sub>2</sub> was removed to fully dry the hydrogels. The gels were dried and grinded into fine powders. The conductivity was measured by a Vernier CON-BTA conductivity meter and the data was collected by LABQuest® 3. The probe of the conductivity meter was fully dipped in the solution of the ZnCl<sub>2</sub>-cellulose mixture containing AA and MBA. The aqueous solution of APS was quickly added into the vial under stirring in about 5 s. The mixture was set back to the steady state and the conductivity was collected. X-ray powder diffraction (XRD) patterns were collected using a Theta - Theta X-ray diffractometer (Rigaku Corporation). The diffraction angle of 2θ ranged from 5° to 85°. For <sup>13</sup>C NMR, crystalline cellulose and the film samples were packed in a 4 mm Zirconia rotor and spun at 5 kHz, and run on a Bruker AVANCE III 400 WB, operating at 100 MHz for <sup>13</sup>C. Data was acquired on a 4 mm HXY CPMAS probe as a cross-polarization of spinning sidebands (CP) for clarity at 300 K with a 55 kHz decoupling field and 2.0 ms of contact time. SEM (Phenom XL G2 SEM) was used to analyze the microstructure and surface morphology of lyophilized hydrogel samples under an accelerating voltage of 10 kV after spraying with gold. Rheological analysis was determined by a rheometer (MCR 302, Anton Paar) equipped with a parallel palate (25.0 mm diameter). Oscillatory frequency measurements were performed in a condition of 0.1-100 rad/s angular frequency at a fixed strain of 1% at 25 °C. Mechanical tests were carried out on the hydrogels/films using a TA-XT plus C texture analyzer (Stable Micro Systems) equipped with a 50 kg load cell at a speed of 2 mm/s and the stress values were calculated by Exponent software (Stable Micro systems, UK). To rehydrate the film, a dry film was incubated in a desiccator under controlled humidity monitored by a hydrometer (Govee Smart Thermo H5100) and the film sample was left in the desiccator at lease for 3 h to be rehydrated under a desired humidity.

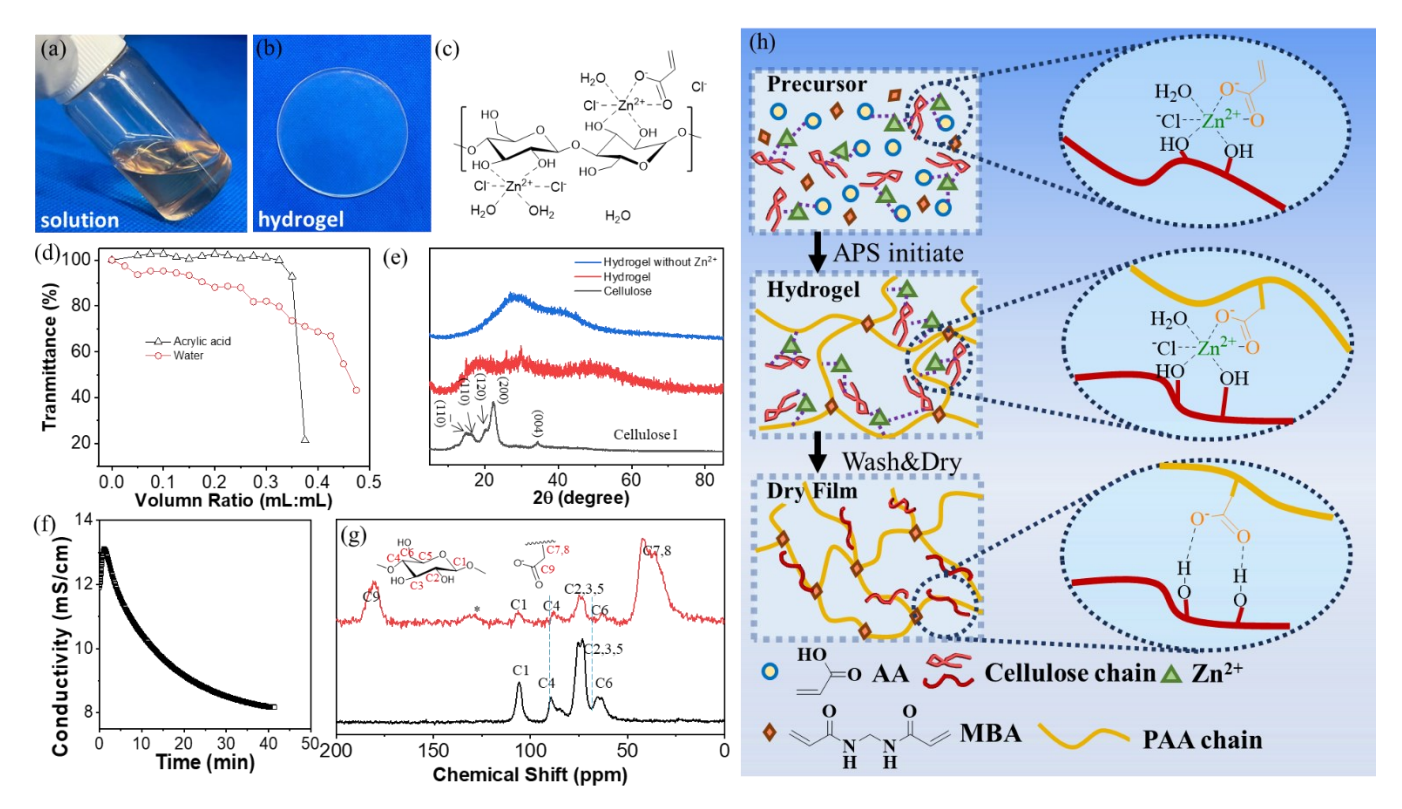


**Figure 1.** (a,b) Pictures of cellulose solution (3 wt% dissolved in 70 wt% ZnCl<sub>2</sub> in water, a) and freshly prepared hydrogel (C2.5/PAA14.9, diameter of 10 cm, b). (c) Chemical structure illustrating interaction among cellulose, Zn<sup>2+</sup> and acrylic acid. (d) Transmittance measurement of 3 wt% cellulose solution at 750 nm after addition of different amounts of acrylic acid (black) or water (red). (e) XRD patterns for cellulose microcrystal powder (black), C2.5/PAA14.9 gel (red), and C2.5/PAA14.9 gel after removing Zn<sup>2+</sup> (blue). (f) Conductivity changes during the preparation of C2.5/PAA14.9. (g) Solid <sup>13</sup>C NMR of pure cellulose (black) and C2.5/PAA14.9after removing Zn<sup>2+</sup> (red). The peak marked with \* is due to the spinning sideband of PAA. (h) Scheme of cellulose hydrogel/film formation and molecular interactions.

# 3. Results and Discussion

Cellulose microcrystals were first dissolved in ZnCl<sub>2</sub>. The molten salt hydrate of ZnCl<sub>2</sub>·3H<sub>2</sub>O can dissolve cellulose microcrystals upon gentle heating at 65 °C.<sup>27</sup> Figure 1a shows a cellulose solution in the molten salt hydrate of ZnCl<sub>2</sub>·3H<sub>2</sub>O with a weight ratio of 3 wt%. The solution was highly viscous and slightly yellowish, due to the partial oxidations of hydroxyl groups during dissolution. The cellulose microcrystal was fully dissolved in ZnCl<sub>2</sub> solution through the breaking of interchain hydrogen bonds and new coordination with Zn<sup>2+</sup> ions. The ZnCl<sub>2</sub>-cellulose mixture was sensitive to the change of solvent, *e.g.*, the number of water molecules in the coordination sphere of Zn<sup>2+</sup> ions. Previous literature suggests that

the molten salt hydrate of ZnCl<sub>2</sub> with two or three water molecules was able to dissolve cellulose.<sup>25</sup> Upon dilution of the ZnCl<sub>2</sub>-cellulose mixture with water, the solution quickly became opaque with the increase of water concentration as seen from the sharp drop in transmittance in the titration curve in Figure 1d. Since the solution had a high viscosity, the addition of water causes the local precipitation of cellulose that could not be re-dissolved even under stirring. AA, on the other hand, did not disrupt the solubility of cellulose. The titration of AA to the ZnCl<sub>2</sub>-cellulose mixture reached 30.0 vol% without precipitation of cellulose. AA as an acid can bind with Zn<sup>2+</sup> ions likely by replacing Cl<sup>-</sup> ions without disrupting the coordination between Zn<sup>2+</sup> and cellulose or changing the polarity of the solvent.

After mixing the ZnCl<sub>2</sub>-cellulose and AA in the presence of MBA as a cross-linker and APS as a radical initiator, the solution mixture was quickly degassed and transferred to a petri dish with a glass slide cover on the top. We first followed the gelation through the conductivity change during polymerization (Figure 1f). The mixture was ionically conductive with a conductivity of 12 mS/cm, due to the presence of free Zn<sup>2+</sup> ions in solution. Once the polymerization was initiated, the conductivity first increased. This was likely due to the release of Zn<sup>2+</sup> ions only bounded with AA once polymerized. After the induction period of 1.2 min, there was a continuous decrease of the conductivity, due to the increase of viscosity. After 30 min, the conductivity plateaued, suggesting the formation of ionic gels. To reach a high conversion of AA, polymerization was carried out about 2 h to yield transparent ionic hydrogels.

Figure 1e shows the X-ray diffraction (XRD) pattern of cellulose microcrystals and hydrogels of C2.5/PAA14.9. Cellulose microcrystals are highly crystalline cellulose I with distinct peaks at 14.5° for (110), 16.5° for (110), for 22.5° (200) and 34.5° for (004). However, hydrogels did not show any obvious diffraction peaks but broad humps, indicating that cellulose was still well-bound with Zn<sup>2+</sup> ions and likely solvated. To examine the interaction of cellulose and PAA, we further removed ZnCl<sub>2</sub> by thoroughly washing with water. Without ZnCl<sub>2</sub>, the hydrogel still did not show any diffraction peaks, suggesting that cellulose was amorphous. We further dried the hydrogels and used solid state <sup>13</sup>C NMR spectroscopy to investigate the crystalline state of cellulose (Figure 1g). The original cellulose powder shows well-resolved peaks for C1-C6. Both C4 and C6 had a shoulder peak at a lower chemical shift as an indication of amorphous cellulose. In the dried hydrogel film after the removal of ZnCl<sub>2</sub>, the <sup>13</sup>C resonance peaks at ca. 180 ppm and 30-40 ppm are well-defined for the carbonyl and methylene groups of the PAA backbones, respectively. While all resonance peaks for cellulose C1-C6 were well-preserved, the peaks of C4 and C6 were significantly narrowed, and their main peaks at higher chemical shift disappeared. This is evidence

for the change of cellulose packing structures in the composite with PAA that inhibits the formation of crystalline cellulose.

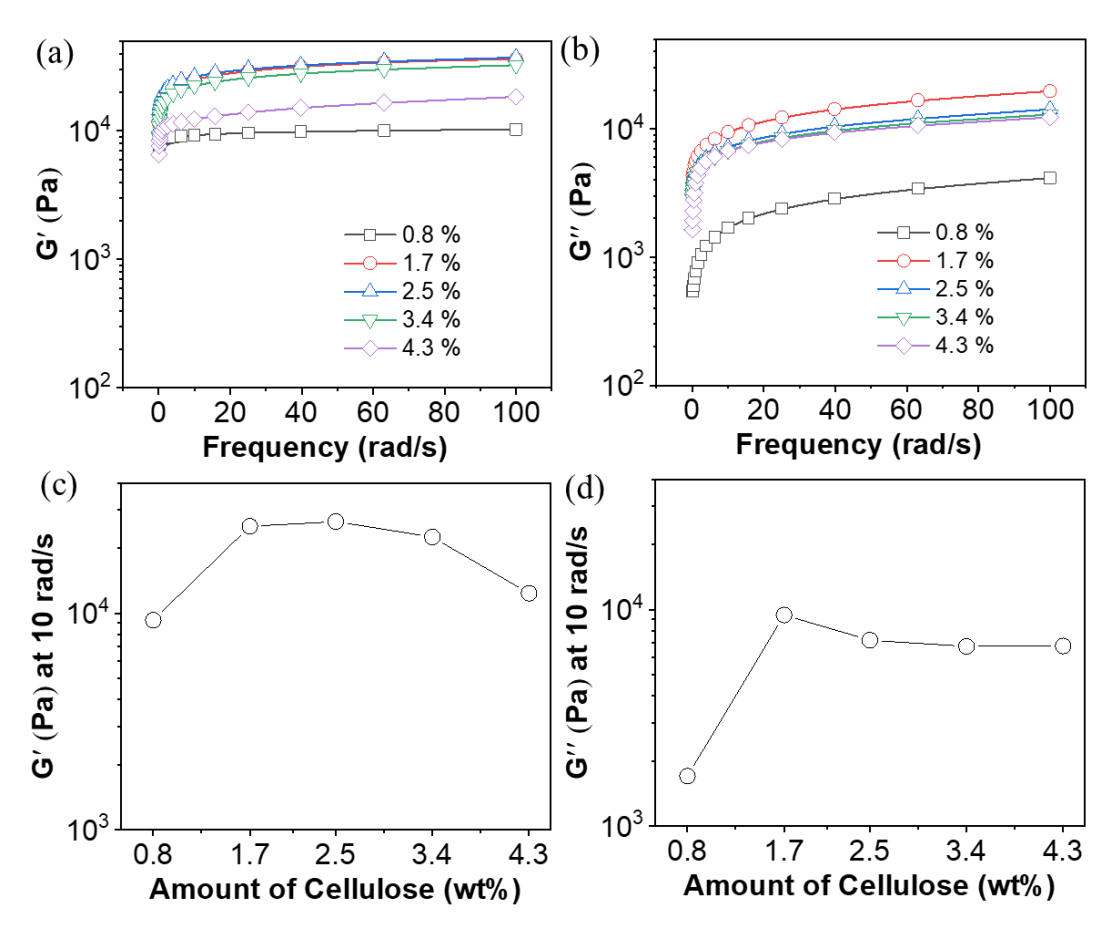
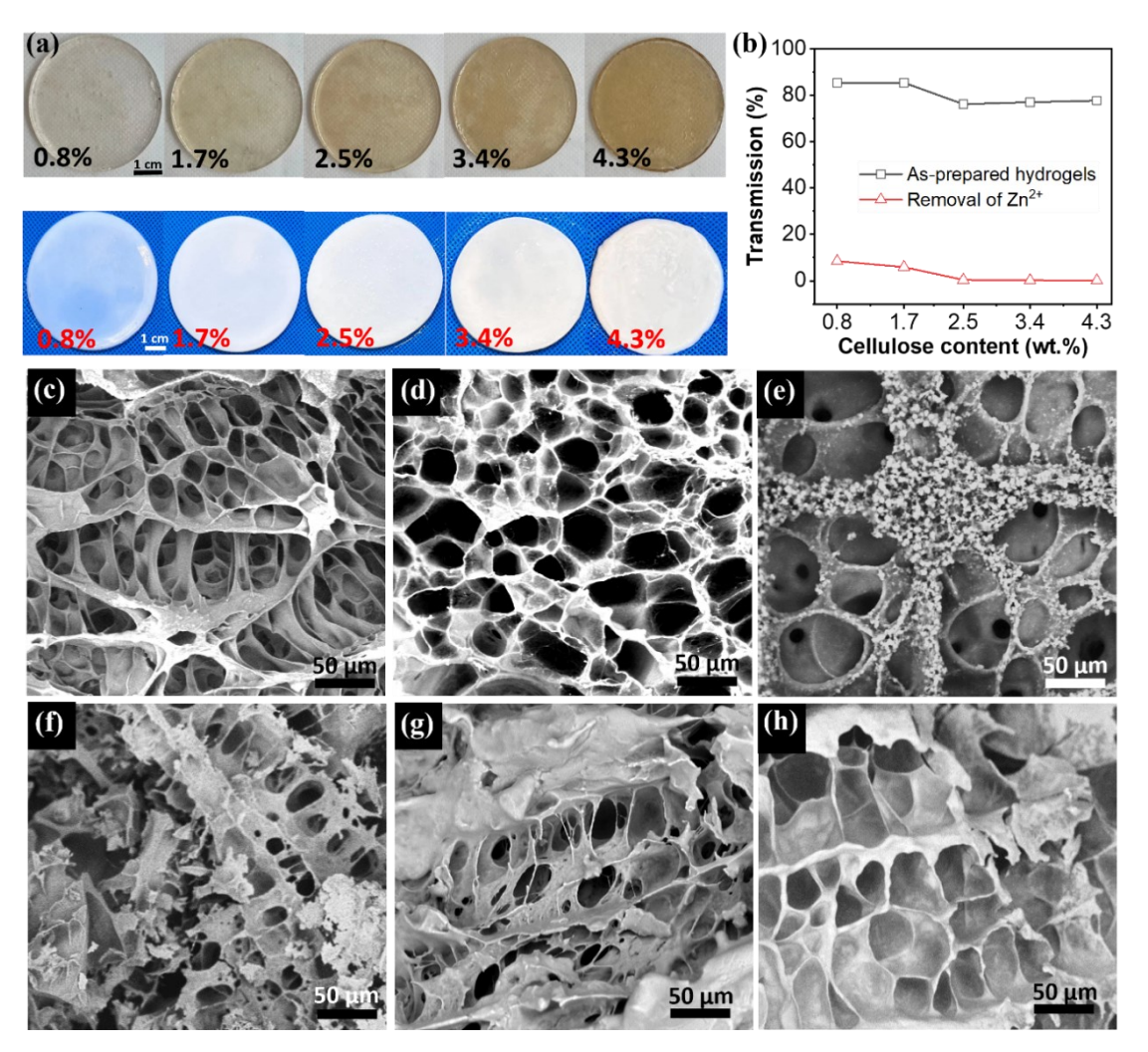


**Figure 2.** Rheology properties of cellulose/PAA gels. (a) Storage modulus (G') and (b) loss modulus (G'') plotted with different concentrations of cellulose with the same concentration of PAA (14.9 wt%). The gel was subjected to a small oscillation strain (1%) at an oscillation frequency from 0.1 to 100 rad s<sup>-1</sup>. (c) Storage modulus (G') and (d) loss modulus (G'') at 10 rad s<sup>-1</sup> with different amounts of cellulose in the gel corresponding to (a) and (b).

The shear moduli of the C2.5/PAA14.9 hydrogel were investigated using a dynamic frequency sweep in rheology. The gel samples were cut into disk shapes with a diameter of 25 mm. A small angle oscillating shear measurement at a strain of 1% was used to determine storage modulus (G') and loss modulus (G"), within a frequency range of 0.1 to 100 rad/s (Figure 2). C2.5/PAA14.9 has a G' of 26 kPa and G" of 7 kPa, corresponding to a loss factor (G"/G') of 0.27. This is indicative of the formation of hydrogel networks. The viscoelastic moduli within the whole frequency are strongly dependent on the

covalent network formed by polymerization of AA. Lowering the content of PAA in the hydrogel would result in the loss of mechanical robustness. For example, by decreasing PAA to 9.0 wt%, the G' of ionic hydrogels fall to 4 kPa (see Figure S1). The amount of cellulose, on the other hand, has less impact on the moduli. With cellulose concentrations in the range of 0.8 wt% to 4.3 wt%, the G' of ionic hydrogels ranged from 10 kPa to 30 kPa.

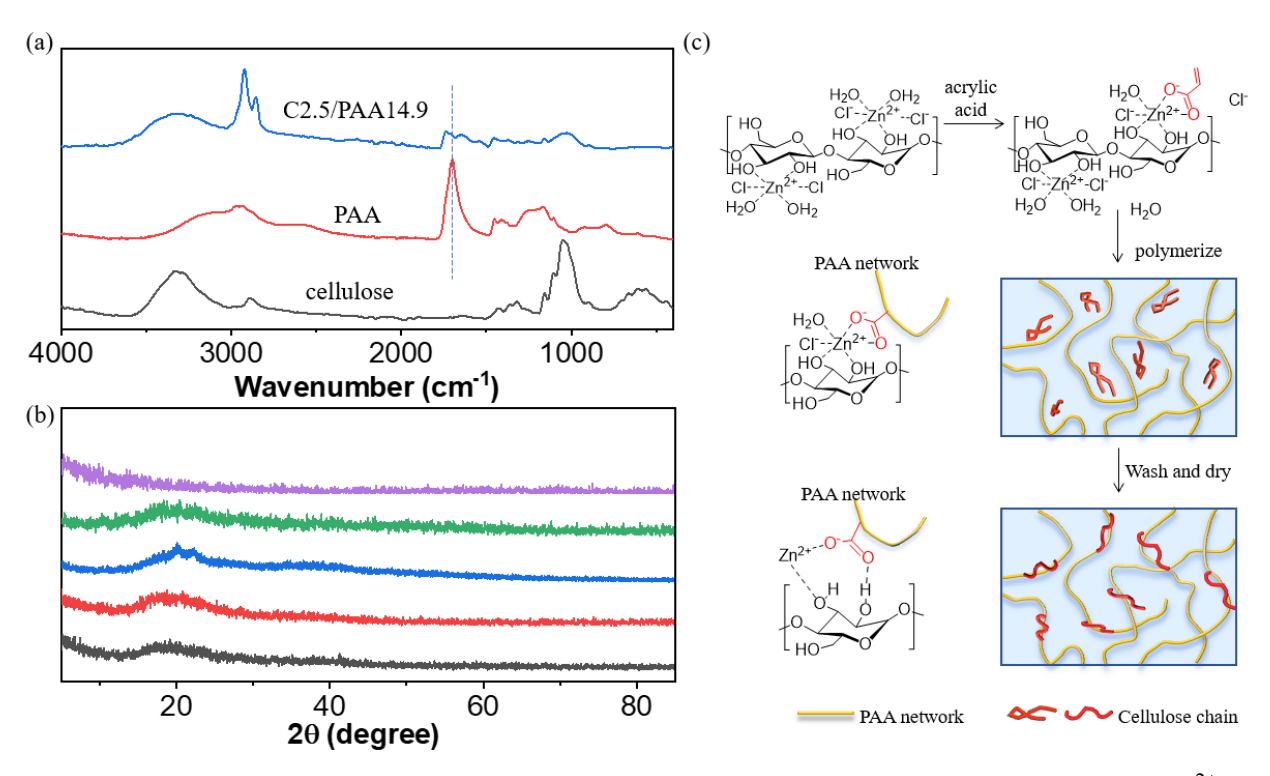
The ionic gels of cellulose/PAA are mostly transparent with a slightly yellowish color (Figure 3a). The transmittance of hydrogels is >70% across all cellulose and PAA concentrations (Figures 3b and S2). The hydrogels were further lyophilized for structural and spectroscopic characterizations. To do so, ZnCl<sub>2</sub> was removed by washing with water. Upon the removal of ZnCl<sub>2</sub>, the ionic gels became opaque and their transmittance decreased dramatically (Figures 3b). There was a clear volume expansion of hydrogels as the water swells PAA. The change of transmittance is due to the solvation state of cellulose. The removal of ZnCl<sub>2</sub> results in the collapse of cellulose chains (water as a non-solvent for cellulose), where the solubilized cellulose crashed out within hydrogel and form a hydrogen bonding network on top of the covalently cross-linked PAA network. The diffusion of ZnCl<sub>2</sub>, however, is not uniform across the film. With a faster exchange at the interface of ionic gels and water, cellulose would likely have a higher accumulation at the surface of hydrogels, which gives rise to opaqueness after removal of ZnCl<sub>2</sub>. Cellulose/PAA composite films became transparent after drying (Figure S3). The films are apparently homogeneous, comparable to those films made of nanocelluloses. Note that, after incubating in water overnight, there is still residual ZnCl<sub>2</sub> in the film. About 5 wt% of ZnCl<sub>2</sub> relative to the total weight of the film was found from X-Ray fluorescence spectroscopy (see Figure S4). The residual ZnCl2 is likely bound with PAA and cellulose through ionic interaction. We assume that strongly bound ZnCl<sub>2</sub> improves the interface of PAA/cellulose and allows cellulose to interact with the PAA network.



**Figure 3.** Images of the gels. (a) Optical images of cellulose/PAA gel with different amounts of cellulose before (top) and after (bottom) removal of Zn<sup>2+</sup>. (b) Transmittance of hydrogels with different amounts of cellulose at 750 nm before (black) and after (red) removal of Zn<sup>2+</sup>. SEM images of (c) C0.8/PAA14.9, (d) C1.7/PAA14.9, (e) C2.5/PAA14.9, (f) C3.4/PAA14.9, (g) C4.3/PAA14.9 and (h) C2.5/PAA16.7.

Figures 3c-h show typical SEM images of PAA/cellulose hydrogels after removal of ZnCl<sub>2</sub> and lyophilization. Figures 3c to 3g are the hydrogel samples with cellulose content ranging from 0.8 wt% to 4.3 wt%. All hydrogels are highly porous. The pore size is not uniform in the range of tens to hundreds of µm. However, the increase in cellulose content dramatically changes the surface structures of hydrogel pores. The hydrogel with the lowest concentration of cellulose (C0.8/PAA14.9) has a smoother surface, where cellulose particles are tightly attached to the PAA framework (Figure 3c). With the increase of cellulose to 2.5 wt%, there are cellulose nanoparticles and microparticles formed and visible on the pore

surface of the PAA network (Figure 3e). It is notable that all cellulose particles formed on the top of the PAA network as a "sandwich" structure, and nearly no cellulose islands were observed under SEM. This was presumably attributed to the hydrogen bonding between cellulose and PAA that allowed the high local concentration of cellulose to nucleate and grow. The further increase of cellulose concentration in hydrogels increases the layer thickness of cellulose particles, where a dense layer of cellulose was observed in Figures 3f and 3g. We noted that the structures were dominated by the relative ratio of PAA/cellulose. The increase of PAA decreases the pore size, but the well-dispersed cellulose particles could be seen even at higher concentrations. C2.5/PAA16.7 as an example in Figure 3h has a much denser network, but no obvious large cellulose particles are seen in SEM. Those microstructural changes can be correlated to the physical states of hydrogels, *e.g.*, transmittance. When increasing the concentration of PAA, hydrogels showed a higher transmittance (see Figure S4).



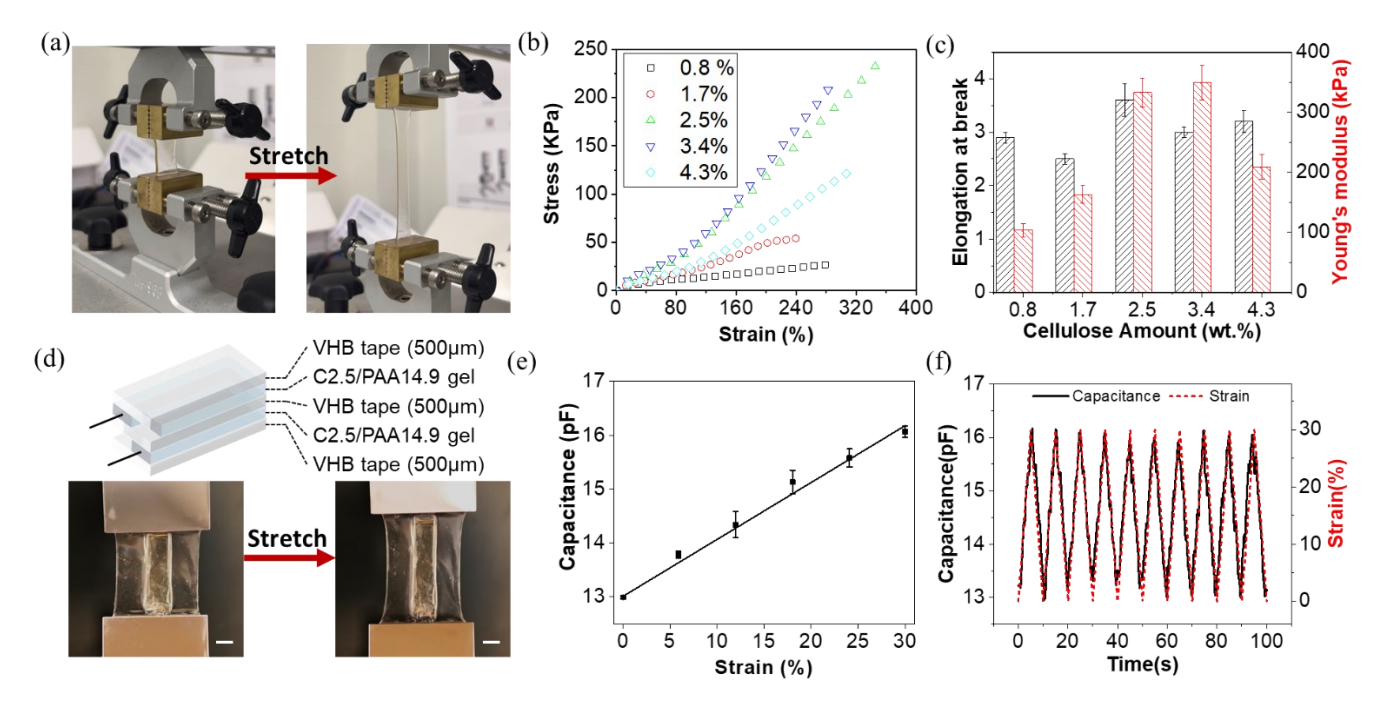
**Figure 4.** (a) FT-IR of pure cellulose (black), PAA (red) and C2.5/PAA14.9 with removal of Zn<sup>2+</sup> (blue). (b) XRD pattern of C0.8/PAA14.9 (black), C1.7/PAA14.9 (red), C2.5/PAA14.9 (blue), C3.4/PAA14.9 (green), C4.3/PAA14.9 (purple) with removal of Zn<sup>2+</sup>. (c) Schemes of cellulose binding changes with PAA network in process of polymerization and removal of Zn<sup>2+</sup>.

Figure 4a shows the FT-IR spectra of PAA/cellulose films. In pure cellulose, the C-O stretching band at 1046 cm<sup>-1</sup> and a weak C-H stretching band at 2892 cm<sup>-1</sup> are representative of cellulose, along with the β-glycosidic linkage between glucose units at 898 cm<sup>-1</sup>. A broad O-H stretching peak is also evidenced for the strong hydrogen bonding of cellulose. In pure PAA, a similar C-H stretching was seen at 2930 cm<sup>-1</sup> that is covered by the broad peak of the O-H stretching. A distinct peak at 1698 cm<sup>-1</sup> was assigned for the C=O stretching. In the PAA/cellulose composite, the C=O stretching appeared as a doublet peak with a lower shoulder at 1682 cm<sup>-1</sup> and a higher one at 1734 cm<sup>-1</sup>. The two forms of C=O stretching suggest the multiple levels of interaction, including the hydrogen bonding between C=O and cellulose that lowers the C=O stretching frequency and the ionic interaction with Zn<sup>2+</sup> that increases the C=O stretching frequency.<sup>32</sup> Figure 4b shows XRD pattern of PAA/cellulose film at different concentrations of cellulose. All films show typical features of amorphous humps. With the SEM images, this likely occurs due to the presence of PAA and Zn<sup>2+</sup> that inhibit the crystallization of cellulose.

Figure 4c illustrates a possible mechanism in the interchange of molecular interactions between PAA and cellulose. The original cellulose microcrystals were first dissolved in ZnCl<sub>2</sub> by breaking hydrogen bonds among crystalline cellulose, while adding coordination bonds among Zn<sup>2+</sup> ions and the hydroxyl groups of cellulose. AA, as an acid to form ionic bonding with Zn<sup>2+</sup> ions, likely competes with Cl<sup>-</sup> ions while also did not disrupt the binding between Zn<sup>2+</sup> ions and cellulose at a low concentration. On the other hand, adding water disrupts interaction between Zn<sup>2+</sup> ions and cellulose to precipitate cellulose from the ZnCl<sub>2</sub>-cellulose mixture (Figure 2c). After formation of hydrogels, the network of PAA interlocks cellulose with ZnCl<sub>2</sub> to bridge the two polymers. With the chemical cross-linking of PAA and the coordination interaction of ZnCl<sub>2</sub>, the interpenetrated hydrogels are elastic and stretchable (see below). Upon washing and drying, cellulose that is not water-soluble precipitates out in the hydrated network of PAA. Therefore, cellulose formed particles anchored on the network of PAA through hydrogen bonding and ionic interaction of residual ZnCl<sub>2</sub>. Those cellulose particles were likely amorphous or nanocrystalline because of the interaction between PAA and cellulose to inhibit the crystallization, as suggested by the XRD results (Figure 4b).

The interpenetrated ionic gels were not only ionically conductive but also physically strong, highly stretchable and compressible. To measure their mechanical properties, all ionic gels (concentration range:  $0.8 \sim 4.3\%$ ) were cut into strips with a dimension of 30 mm×10 mm with a thickness of 1 mm. A typical tensile stretching of the C2.5/PAA14.9 hydrogel is shown in Figure 5a as an example and typical stress-strain curve of ionic gels with different cellulose amount are given in Figure 5b. The C2.5/PAA14.9 gel

was stretchable with an elongation at break up to 363% and a fracture strength of up to 246.5 kPa and a Young's modulus of 332.7 kPa. The gel toughness, defined as the area under stress-strain curve, is 39.7 MJ/cm<sup>2</sup>. The further increase of the cellulose concentration to more than 2.5% does not improve the elongation at break. All hydrogels with the cellulose amount in the range of 0.8% to 2.5%, their maximum elongation is around 300%; but a slightly higher Young's modulus was seen Figures 5b and c.



**Figure 5**. Mechanical characterizations of ionic hydrogels and strain sensors. (a) Pictures of ionic gels under tensile stress. (b) Stress-strain curves of ionic gels at different amounts of cellulose. (c) Elongation at break and Young's modulus of ionic gels at different amounts of cellulose. (d) Scheme of the strain sensor and images of the sensor before and after stretching. (e) Capacitance of the sensor as a function of strain under stretching. (f) Capacitance of the strain sensor over cyclic loading.

These stretchable ionic hydrogels can be used for capacitive strain sensors. As schematically illustrated in Figure 5d, the capacitive strain sensor is composed of two ionic gel layers as the two conductive electrodes, and the VHB tape as the dielectric elastomer (center layer) between the two electrodes. The sensor is further encapsulated with VHB from the top and bottom as barriers to fluids. The strain sensor was affixed to a mechanical tester (see the supporting video) and stretched to 30% strain. Subsequently, the performance of the strain sensor was evaluated through the cyclic loading at a

frequency of 0.1 Hz (a cycle of stretching and release). Figure 5e and 5f demonstrate a strong correlation between the capacitance change and the applied strain, and high repeatability over 10 cycles. With the change of the strain between 0–30% (red dots), the capacitance correspondingly followed the trend between 13.0–16.1 pF with a good reproducibility. To assess the performance of ionic hydrogel-based sensors for potential applications on curvilinear surfaces, we also tested the sensors at bending angles ranging from 0° to 180° (Figure S5). The sensors exhibited relative capacitance changes of less than 1.5% during bending to 180°, demonstrating their large flexibility and robust sensing capabilities when operated under curved conditions.

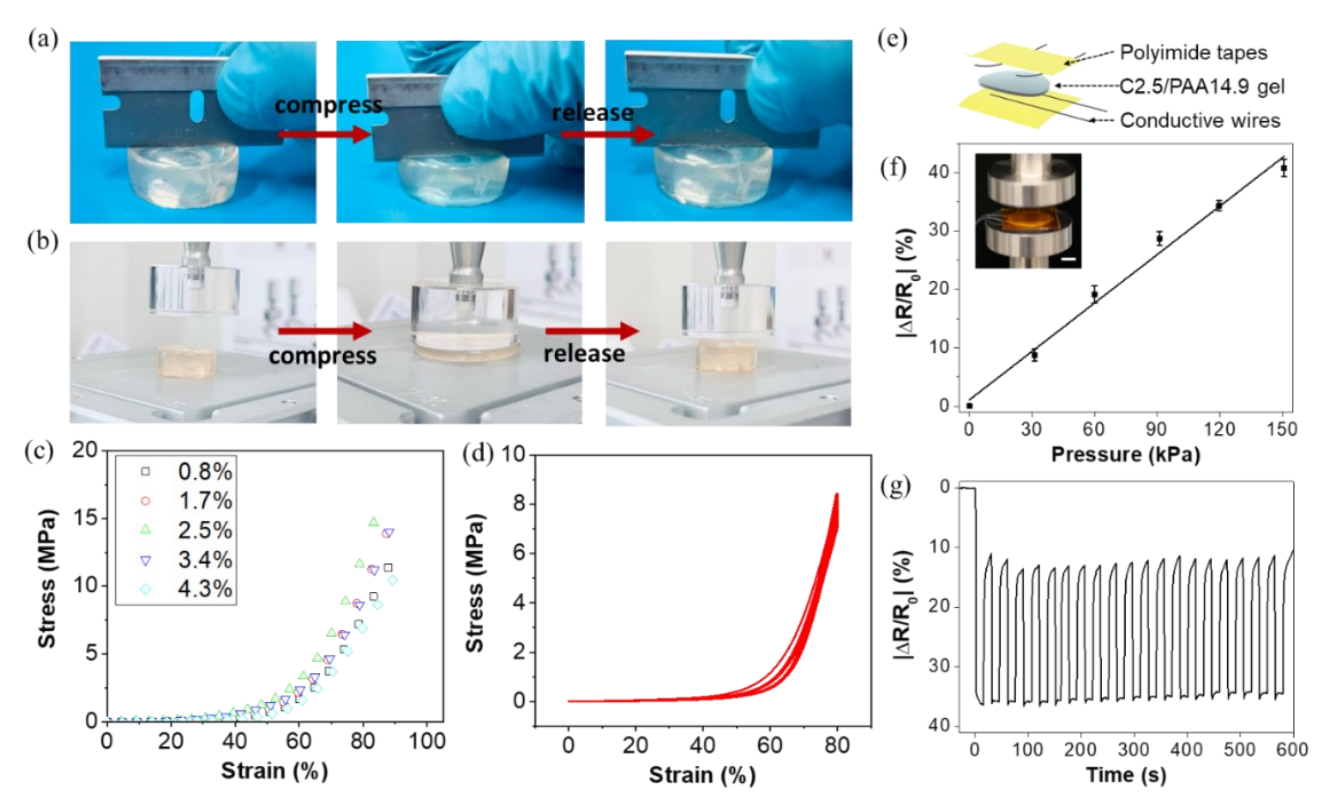


**Figure 6.** Compression tests of ionic hydrogels and characterizations of resistive pressure sensors fabricated from ionic hydrogels. (a,b) Pictures of C2.5/PAA14.9 ionic gels with a blade or loading press on the surface and recovery. (c) Compression stress-strain curves of ionic gels at different cellulose amounts. (d) A typical successive loading-unloading compression test of C2.5/PAA14.9 gel for 20 cycles at 80% strain without resting intervals. (e) Scheme of the pressure sensor. (f) Resistance changes of the pressure sensor as a function of applied pressures. The inset is a photo showing the pressure sensor under a mechanical testing setup. (g) Cycling loading of the pressure sensor.

Cellulose/PAA ionic hydrogels were highly compressible and very tough to resist compressive force. With a razor blade applied on the surface, the ionic hydrogels were not easily cut to pieces, and they could fully recover back to their original forms after a blade was pressed on the surface (Figure 6a). Under a compression test of up to 80% deformation, ionic hydrogels also recovered back to their original forms with mechanical fracture (Figure 6b). The typical compressive stress-strain curves are given in Figures 6c and S6. With increasing the amount of cellulose from 0.8 to 2.5%, the ionic gels showed an increase of their compressive stress. At 83% of strain, the compression stress is 14.7 MPa for C2.5/PAA14.9, while it was 11.4 MPa for C0.8/PAA14.9. With increasing of the PAA content in the gel, the compression stress of the C2.5/PAA16.7 could reach ~20 MPa (Figure S6). Under successive loading-unloading compression tests, the C2.5/PAA14.9 ionic gel had a highly reproduceable stress-strain curve. The rapid recovery of original shape after undergoing a series of compressive deformations of 80% and subsequently releasing force was seen after 20 cycles in Figure 6b. This suggests that the ionic network formed by ZnCl<sub>2</sub> between cellulose and PAA could rapidly dissipate the mechanical energy exerted on hydrogels without mechanical fracture.

Those ionic gels could further be used for pressure sensing. To fabricate the pressure sensor, the C2.5/PAA14.9 ionic gel was cut into a circular geometry with a diameter of 15 mm. Two pairs of orthogonal carbon conductive threads were laid across the circular ionic gel (Figure 6e). Finally, the polyimide tape (60 µm) was used to encapsulate the sensor as barriers to fluids. Figure 6f presents a good linear relationship between the resistance change of the pressure sensor and the applied pressure, with R<sup>2</sup>=0.9966. A cyclic test was further performed under a constant displacement mode, where a load of 120 kPa was applied to the pressure sensor for 20 cycles (Figure 6g). The pressure sensor has shown high repeatability over the cyclic test, with the relative resistance changes maintaining at 35% under 120 kPa over 20 cycles.

Cellulose and their composite films are usually brittle. For example, papers made of regenerated cellulose microcrystals with a fibrous network are not stretchable and their elongation at break is often below 5%, where strongly hydrogen bound cellulose microcrystals cannot dissipate the mechanical energy through their crystalline domains.<sup>33</sup> To prepare cellulose/PAA composite films, we removed ZnCl<sub>2</sub> from hydrogels by rinsing with water and dried them under vacuum. With the presence of amorphous cellulose, those films are semi-transparent (~50% transmittance at 750 nm with a thickness of 0.2 mm). A typical transmission plot is given in Figure S4. Fully dried cellulose/PAA films are brittle as well. Figure 7a shows a typical stress-strain curve of the C2.5/PAA14.9 film. It has a very high Young's modulus of 4.1

GPa in the dried state under ambient air environment, comparable to that of reported nanocellulose films.<sup>34</sup> The film is not stretchable, and it failed mechanically at  $\sim$ 1% elongation.

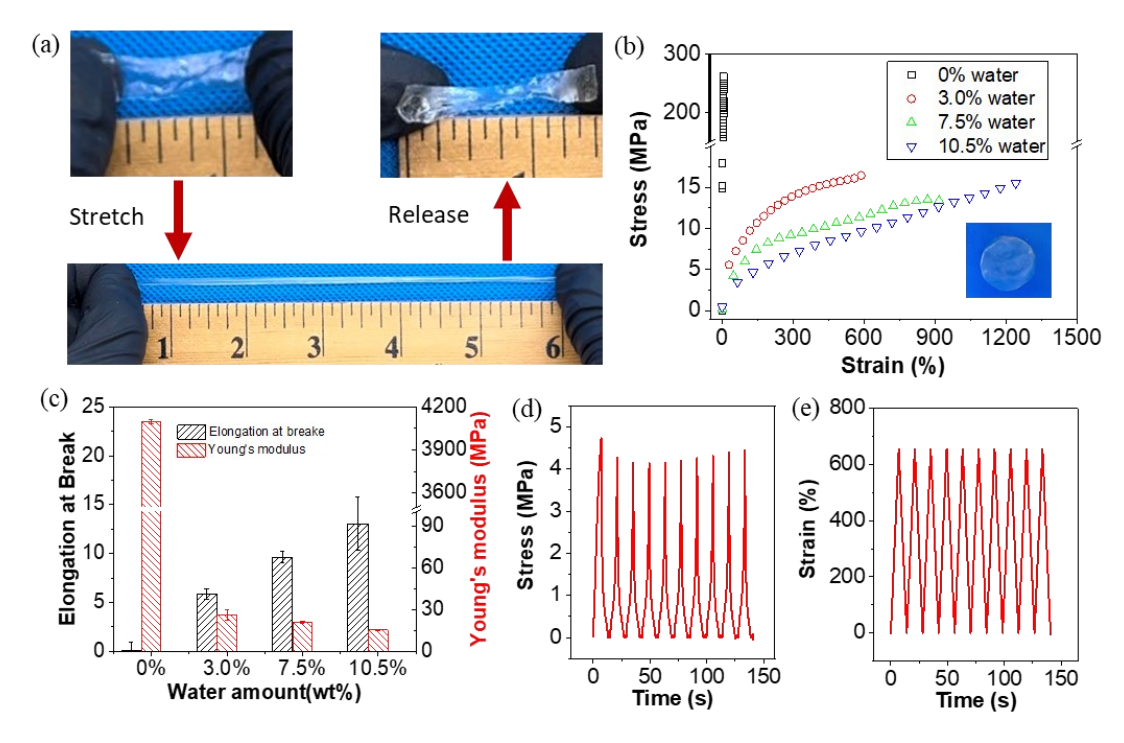


**Figure 7**. (a) Images of C2.5/PAA14.9 films under mechanical stretching. (b) Tensile stress-strain curves of rehydrated C2.5/PAA14.9 film having different water amounts (Inset: an optical image of rehydrated film). (c) Elongation at break and Young's modulus of C2.5/PAA14.9 film at different amounts of water. (d) Stress changes in a typical cyclic loading-unloading tensile test of C2.5/PAA14.9 rehydrated film for 10 cycles at 650% strain without resting intervals. (e) Strain changes in a typical successive loading-unloading tensile stress tests of the C2.5/PAA14.9 rehydrated film for 10 cycles at 650% strain without resting intervals.

After rehydrating under humidity, the cellulose/PAA film showed a dramatic change in their mechanical behaviors, *e.g.*, becoming highly elastic (Figure 7a). The C2.5/PAA14.9 film could be rehydrated and uptake up to 10.5 wt% moisture (through gravimetric analysis) under 100% humidity at room temperature for 3 h, very similar to that of regenerated cellulose papers with saturated water uptake in air. Under mechanical stretching, the film was elastic with an elongation at break of 1300%. The film with tensile strength of 15.7 MPa was mechanically as strong as paper but as elastic as natural rubber (Figure 7b). The film is highly elastic as confirmed by the stress-time and strain-time plots for 10 cycles

with a constant strain of 600% in Figures 7d and e. At a constant strain, the stress in each cycle is very similar, suggesting the fast recovery of their deformation. The mechanical strength of the film was dominated by its moisture content. The impact of the moisture content in cellulose/PAA films on their mechanical performance was investigated by incubating the film with moist air at different times. With 3% and 7.5% of moisture content, similar elastic but tough films were produced (Figure 7c). The tough elastic films showed a steep linear plastic region observed at the initial strains up to 80%, followed by a yielding behavior at a higher strain. The films could still be stretched to > 600% strain.

The impact of humidity on the mechanical strength of cellulose/PAA composite films are given in Figure 8a. The film of C2.5/PAA14.9 was incubated under desired humidity from ~30% to 100% for 3 h. The film became more elastic where the elongation increased from ~6% to ~1300% with a higher humidity, similar to those films with different water contents. The decrease of Young's modulus from 4.1 GPa to 15.4 MPa was also seen after rehydration under different humidity (Figure 8b). To further confirm the elastic deformation, cellulose/PAA films with different cellulose and PAA contents were also investigated (Figures 8c-d and S7). All films were highly stretchable after rehydration. Their Young's modulus varied in the range of 7-15 MPa and the elongation at break varied in the range of 600%-1300%. Furthermore, the rehydration process is also repeatable under drying/rehydration cycles. The mechanical property of the rehydrated film had a minimum change after five drying/rehydration cycles (Figure 8d). The elastic behavior of cellulose composites is unique. Their mechanical properties have been cross-compared with the reported values in literatures (Figure 8e and Table S1). 35-47 The composite films show high mechanical strength as cellulose films but also high elasticity as their hydrogels. The high elasticity is likely endowed by the amorphous nature of cellulose in the composite where hydrogen bonding among cellulose strands and hydrated PAA with residual  $Zn^{2+}$  ions can provide abundant sites to dissipate mechanical energy.<sup>48</sup>

To demonstrate the potential application of the cellulose/PAA composite film, we prepared strain sensors. Given the residual Zn<sup>2+</sup> ions and low density/water content as printing paper, such composite film can still work as electrodes for the wearable strain sensors. The typical sensor configuration is shown in Figure 8e. Those sensors were mounted on a human hand model to monitor the finger joint bending and extending states (Figures 8e and f). With the lighter weight and better processibility as compared to hydrogels, the sensor area with the cellulose/PAA composite film was reduced by five times, and the overall thickness was decreased to 60% of the hydrogel device (Figure 5). The strain sensors show outstanding conformability and optical transparency (Figure 8f). In addition, the real-time

capacitance changes showed stable performance, while the finger was repeatedly bent and extended (Figure 8g). Those composite films can potentially expand versatility in wearable sensor applications.

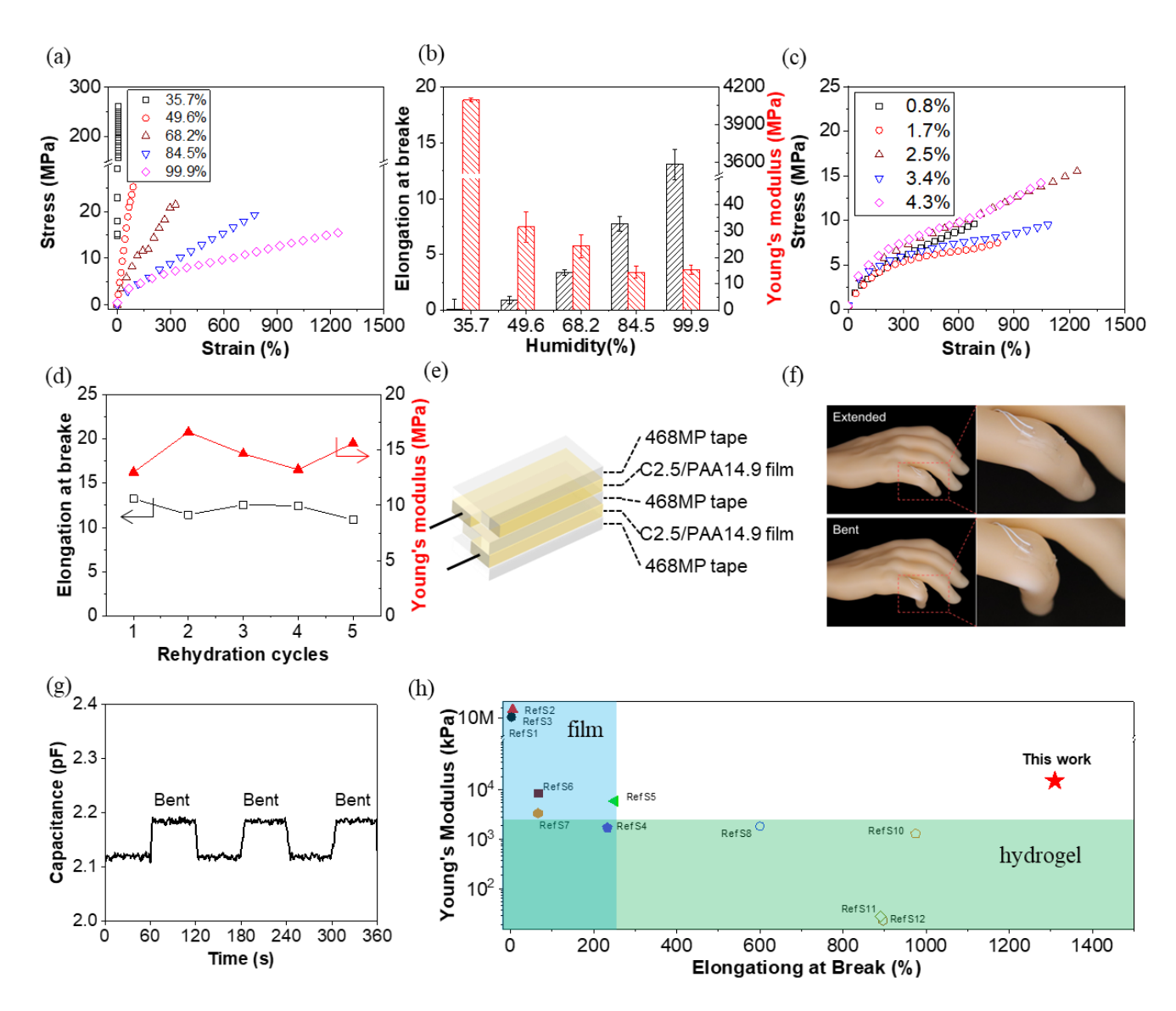


**Figure 8**. (a) Tensile stress-strain curves of rehydrated C2.5/PAA14.9 film under different humidity. (b) Elongation at break and Young's modulus of C2.5/PAA14.9 film under different humidity. (c) Tensile stress-strain curve of rehydrated cellulose/PAA films with different cellulose amounts and with about 10 wt% of moisture in films. (d) Elongation at break and Young's modulus of C2.5/PAA14.9 film under five drying/rehydration cycles. (e) Scheme of the film strain sensor. (f) Image demonstration and (g) real-time capacitance change of strain sensors with film electrodes mounted on the finger joint in both extended and

bent states. (h) Comparing rehydrated C2.5/PAA14.9 film with other cellulose-containing hydrogels (open symbols) and films (closed symbols) reported in literature. The references are listed in Table S1.

### 4. Conclusion

We demonstrate a solution process to fabricate porous and amorphous cellulose hydrogels and films. Those cellulose-based materials were designed as composites with synthetic polymers like PAA introduced by *in situ* polymerization of AA in ZnCl<sub>2</sub>-cellulose mixtures. The water-ZnCl<sub>2</sub> mixture solvation system for cellulose had a high tolerance to AA up to 30 vol% without varying the solubility of cellulose in the water-ZnCl<sub>2</sub> mixture. After polymerization, the formation of interpenetrated networks, including the chemical crosslinking of PAA and the ionic/coordination binding among cellulose/PAA and ZnCl<sub>2</sub> formed ionic hydrogels with high mechanical strength. These gels were stretchable, compressible and ionically conductive can be used for wearable sensors to detect mechanical deformation upon stretching and compression. These composite hydrogels can be further dried after the removal of ZnCl<sub>2</sub> to prepare cellulose composite films. With amorphous cellulose, films were semi-transparent and very tough with a Young's Modulus of up to 4 GPa in the absence of water. Their rehydration resulted in the formation of tough but elastic composites. With a water content of 3-10.5 wt%, rehydrated films showed typical characteristics of elastomers with elongation up to 1300%. These new composite films made of synthetic and natural polymers present a workable solution to sustainable materials without compromising their properties.

# **Supporting Information**

Additional rheology results and transmission graphs, FTIR for all the film samples, mechanical properties with different amount of PAA, mechanical properties for all different samples.

#### **Author Contribution**

J. He, X. Wang and J. F. Rusling conceived the idea and co-wrote the first draft. T. Yang carried out the synthesis, characterizations and mechanical tests of the materials. S. Lu and X. Wang worked on assembly of strain/stress sensors and did the measurement. H. Zhu and L. Yang worked on the rheology tests. A. Patetsos, E. McDonald, and M. D. Mellor helped with material characterizations. All authors discussed the results and commented on the manuscript.

# Acknowledgement

JH is grateful for the financial support from the National Science Foundation (CBET 2324346). This work was also partially supported by the Department of Agriculture (USDA) through Award No. 2021-67022-34415, the Research Excellence Program and the Green Emulsions Micelles and Surfactants (GEMS) Center of the University of Connecticut. The authors thank Dr. Nicolas Eddy for his help with the solid NMR measurements.

#### References

- (1) Jiao, Y.; Lu, K.; Lu, Y.; Yue, Y.; Xu, X.; Xiao, H.; Li, J.; Han, J. Highly viscoelastic, stretchable, conductive, and self-healing strain sensors based on cellulose nanofiber-reinforced polyacrylic acid hydrogel. *Cellulose* **2021**, *28*, 4295-4311.
- (2) Miao, Z.; Song, Y.; Dong, Y.; Ge, D.; Shui, J.; He, X.; Yu, H.-Y. Intrinsic conductive cellulose nanofiber induce room-temperature reversible and robust polyvinyl alcohol hydrogel for multifunctional self-healable biosensors. *Nano Research* **2023**, *16* (2), 3156-3167.
- (3) Shen, Y.; Wang, Z.; Wang, Y.; Meng, Z.; Zhao, Z. A self-healing carboxymethyl chitosan/oxidized carboxymethyl cellulose hydrogel with fluorescent bioprobes for glucose detection. *Carbohydrate Polymers* **2021**, *274*, 118642.
- (4) Kamel, S.; A. Khattab, T. Recent advances in cellulose-based biosensors for medical diagnosis. *Biosensors* **2020**, *10* (6), 67.
- (5) Chen, W.; Sun, B.; Biehl, P.; Zhang, K. Cellulose-based soft actuators. *Macromolecular Materials and Engineering* **2022**, *307* (6), 2200072.
- (6) Chen, Z.; Liu, J.; Chen, Y.; Zheng, X.; Liu, H.; Li, H. Multiple-stimuli-responsive and cellulose conductive ionic hydrogel for smart wearable devices and thermal actuators. *ACS applied materials & interfaces* **2020**, *13* (1), 1353-1366.
- (7) Feng, X.; Wang, C.; Shang, S.; Liu, H.; Huang, X.; Jiang, J.; Zhang, H. Multicolor fluorescent cellulose hydrogels actuators: Lanthanide-ligand metal coordination, synergetic color-changing and shape-morphing, and antibacterial activity. *Chemical Engineering Journal* **2022**, *450*, 138356.
- (8) Wu, S.; Yu, F.; Dong, H.; Cao, X. A hydrogel actuator with flexible folding deformation and shape programming via using sodium carboxymethyl cellulose and acrylic acid. *Carbohydrate Polymers* **2017**, *173*, 526-534.
- (9) Dutta, S. D.; Patel, D. K.; Lim, K.-T. Functional cellulose-based hydrogels as extracellular matrices for tissue engineering. *Journal of Biological Engineering* **2019**, *13*, 1-19.
- (10) Pasqui, D.; Torricelli, P.; De Cagna, M.; Fini, M.; Barbucci, R. Carboxymethyl cellulose—hydroxyapatite hybrid hydrogel as a composite material for bone tissue engineering applications. *Journal of Biomedical Materials Research Part A* **2014**, *102* (5), 1568-1579.
- (11) Chen, C.; Xi, Y.; Weng, Y. Recent advances in cellulose-based hydrogels for tissue engineering applications. *Polymers* **2022**, *14* (16), 3335.
- (12) Nath, P. C.; Debnath, S.; Sharma, M.; Sridhar, K.; Nayak, P. K.; Inbaraj, B. S. Recent advances in cellulose-based hydrogels: Food applications. *Foods* **2023**, *12* (2), 350.
- (13) Thivya, P.; Akalya, S.; Sinija, V. A comprehensive review on cellulose-based hydrogel and its potential application in the food industry. *Applied Food Research* **2022**, *2* (2), 100161.

- (14) Zhao, Y.; Zhou, S.; Xia, X.; Tan, M.; Lv, Y.; Cheng, Y.; Tao, Y.; Lu, J.; Du, J.; Wang, H. High-performance carboxymethyl cellulose-based hydrogel film for food packaging and preservation system. *International Journal of Biological Macromolecules* **2022**, *223*, 1126-1137.
- (15) Seth, R.; Page, D. Fracture resistance of paper. *Journal of Materials Science* **1974**, *9*, 1745-1753.
- (16) Xiao, C.; Zhang, Z.; Zhang, J.; Lu, Y.; Zhang, L. Properties of regenerated cellulose films plasticized with α-monoglycerides. *Journal of applied polymer science* **2003**, *89* (13), 3500-3505.
- (17) Shan, C.; Che, M.; Cholewinski, A.; Su, R.; Zhao, B. Multifunctional nanocrystalline cellulose ionogels toward tough and sustainable materials. *Cell Reports Physical Science* **2023**, *4* (8).
- (18) Dandegaonkar, G.; Ahmed, A.; Sun, L.; Adak, B.; Mukhopadhyay, S. Cellulose based flexible and wearable sensors for health monitoring. *Materials Advances* **2022**, *3* (9), 3766-3783. DOI: 10.1039/d1ma01210j.
- (19) Lu, S.-H.; Samandari, M.; Li, C.; Li, H.; Song, D.; Zhang, Y.; Tamayol, A.; Wang, X. Multimodal sensing and therapeutic systems for wound healing and management: A review. *Sensors and Actuators Reports* **2022**, *4*, 100075. DOI: 10.1016/j.snr.2022.100075.
- (20) Jankowska, D. A.; Bannwarth, M. B.; Schulenburg, C.; Faccio, G.; Maniura-Weber, K.; Rossi, R. M.; Scherer, L.; Richter, M.; Boesel, L. F. Simultaneous detection of pH value and glucose concentrations for wound monitoring applications. *Biosens Bioelectron* **2017**, *87*, 312-319. DOI: 10.1016/j.bios.2016.08.072.
- (21) Zhu, Y.; Zhang, J.; Song, J.; Yang, J.; Du, Z.; Zhao, W.; Guo, H.; Wen, C.; Li, Q.; Sui, X.; et al. A Multifunctional Pro-Healing Zwitterionic Hydrogel for Simultaneous Optical Monitoring of pH and Glucose in Diabetic Wound Treatment. *Advanced Functional Materials* **2019**, *30* (6). DOI: 10.1002/adfm.201905493.
- (22) Maia, E.; Peguy, A.; Perez, S. Cellulose organic solvents. I. The structures of anhydrous N-methylmorpholine N-oxide and N-methylmorpholine N-oxide monohydrate. *Acta Crystallographica Section B: Structural Crystallography and Crystal Chemistry* **1981**, *37* (10), 1858-1862.
- (23) Zhu, S.; Wu, Y.; Chen, Q.; Yu, Z.; Wang, C.; Jin, S.; Ding, Y.; Wu, G. Dissolution of cellulose with ionic liquids and its application: a mini-review. *Green Chemistry* **2006**, *8* (4), 325-327.
- (24) Cai, J.; Zhang, L. Rapid dissolution of cellulose in LiOH/urea and NaOH/urea aqueous solutions. *Macromolecular bioscience* **2005**, *5* (6), 539-548.
- (25) Leipner, H.; Fischer, S.; Brendler, E.; Voigt, W. Structural changes of cellulose dissolved in molten salt hydrates. *Macromolecular Chemistry and Physics* **2000**, *201* (15), 2041-2049.
- (26) Fischer, S.; Leipner, H.; Thümmler, K.; Brendler, E.; Peters, J. Inorganic molten salts as solvents for cellulose. *Cellulose* **2003**, *10*, 227-236.
- (27) Chen, Y.; Yu, H.-Y.; Li, Y. Highly efficient and superfast cellulose dissolution by green chloride salts and its dissolution mechanism. *ACS Sustainable Chemistry & Engineering* **2020**, *8* (50), 18446-18454.
- (28) Xi, Y.; Zhang, L.; Tian, Y.; Song, J.; Ma, J.; Wang, Z. Rapid dissolution of cellulose in an AlCl 3/ZnCl 2 aqueous system at room temperature and its versatile adaptability in functional materials. *Green Chemistry* **2022**, *24* (2), 885-897.
- (29) Zhang, X. F.; Ma, X.; Hou, T.; Guo, K.; Yin, J.; Wang, Z.; Shu, L.; He, M.; Yao, J. Inorganic salts induce thermally reversible and anti-freezing cellulose hydrogels. *Angewandte Chemie International Edition* **2019**, *58* (22), 7366-7370.
- (30) Li, K.; Skolrood, L. N.; Aytug, T.; Tekinalp, H.; Ozcan, S. Strong and tough cellulose nanofibrils composite films: mechanism of synergetic effect of hydrogen bonds and ionic interactions. *ACS* sustainable chemistry & engineering **2019**, 7 (17), 14341-14346.

- (31) Wang, M.; Zhang, P.; Shamsi, M.; Thelen, J. L.; Qian, W.; Truong, V. K.; Ma, J.; Hu, J.; Dickey, M. D. Tough and stretchable ionogels by in situ phase separation. *Nature materials* **2022**, *21* (3), 359-365.
- (32) Li, H.; Thanneeru, S.; Jin, L.; Guild, C. J.; He, J. Multiblock thermoplastic elastomers via one-pot thiol—ene reaction. *Polymer Chemistry* **2016**, *7* (29), 4824-4832.
- (33) Eichhorn, S.; Sirichaisit, J.; Young, R. Deformation mechanisms in cellulose fibres, paper and wood. *Journal of Materials Science* **2001**, *36*, 3129-3135.
- (34) Zhao, M.; Ansari, F.; Takeuchi, M.; Shimizu, M.; Saito, T.; Berglund, L.; Isogai, A. Nematic structuring of transparent and multifunctional nanocellulose papers. *Nanoscale Horizons* **2018**, *3* (1), 28-34.
- (35) Qing, Y.; Sabo, R.; Zhu, J.; Agarwal, U.; Cai, Z.; Wu, Y. A comparative study of cellulose nanofibrils disintegrated via multiple processing approaches. *Carbohydrate polymers* **2013**, *97* (1), 226-234.
- (36) Kurihara, T.; Isogai, A. Properties of poly (acrylamide)/TEMPO-oxidized cellulose nanofibril composite films. *Cellulose* **2014**, *21*, 291-299.
- (37) Kumar, V.; Bollström, R.; Yang, A.; Chen, Q.; Chen, G.; Salminen, P.; Bousfield, D.; Toivakka, M. Comparison of nano-and microfibrillated cellulose films. *Cellulose* **2014**, *21*, 3443-3456.
- (38) Lim, D. B. K.; Gong, H. Highly stretchable and transparent films based on cellulose. *Carbohydrate polymers* **2018**, *201*, 446-453.
- (39) Wang, S.; Zhang, X.; Wu, X.; Lu, C. Tailoring percolating conductive networks of natural rubber composites for flexible strain sensors via a cellulose nanocrystal templated assembly. *Soft Matter* **2016**, *12* (3), 845-852.
- (40) Wang, H.; Luo, H.; Zhou, H.; Zhou, X.; Zhang, X.; Lin, W.; Yi, G.; Zhang, Y. Dramatically enhanced strain-and moisture-sensitivity of bioinspired fragmentized carbon architectures regulated by cellulose nanocrystals. *Chemical Engineering Journal* **2018**, *345*, 452-461.
- (41) Wu, S.; Peng, S.; Wang, C. H. Stretchable strain sensors based on PDMS composites with cellulose sponges containing one-and two-dimensional nanocarbons. *Sensors and Actuators A: Physical* **2018**, 279, 90-100.
- (42) Li, L.; Liu, L.; Qing, Y.; Zhang, Z.; Yan, N.; Wu, Y.; Tian, C. Stretchable alkaline poly (acrylic acid) electrolyte with high ionic conductivity enhanced by cellulose nanofibrils. *Electrochimica Acta* **2018**, *270*, 302-309.
- (43) Kobe, R.; Iwamoto, S.; Endo, T.; Yoshitani, K.; Teramoto, Y. Stretchable composite hydrogels incorporating modified cellulose nanofiber with dispersibility and polymerizability: Mechanical property control and nanofiber orientation. *Polymer* **2016**, *97*, 480-486.
- (44) Zhou, Y.; Wan, C.; Yang, Y.; Yang, H.; Wang, S.; Dai, Z.; Ji, K.; Jiang, H.; Chen, X.; Long, Y. Highly stretchable, elastic, and ionic conductive hydrogel for artificial soft electronics. *Advanced Functional Materials* **2019**, *29* (1), 1806220.
- (45) Yang, J.; Han, C.-r.; Xu, F.; Sun, R.-c. Simple approach to reinforce hydrogels with cellulose nanocrystals. *Nanoscale* **2014**, *6* (11), 5934-5943.
- (46) Lee, Y.; Choi, H.; Zhang, H.; Wu, Y.; Lee, D.; Wong, W. S.; Tang, X. S.; Park, J.; Yu, H.; Tam, K. C. Sensitive, stretchable, and sustainable conductive cellulose nanocrystal composite for human motion detection. *ACS Sustainable Chemistry & Engineering* **2021**, *9* (51), 17351-17361.
- (47) Shih, Y.-F.; Lin, S.-H.; Xu, J.; Su, C.-J.; Huang, C.-F.; Hsu, S.-h. Stretchable and biodegradable chitosan-polyurethane-cellulose nanofiber composites as anisotropic materials. *International Journal of Biological Macromolecules* **2023**, *230*, 123116.

(48) Wei, Z.; Duan, H.; Weng, G.; He, J. Metals in polymers: hybridization enables new functions. *Journal of Materials Chemistry C* **2020**, *8* (45), 15956-15980.

# **Table of Contents**

